Desalination and Water Treatment
www.deswater.com

doi: 10.5004/dwt.2020.24981

179 (2020) 288–301
March

Evaluation of microporous acrylic-based activated carbon fibers as novel adsorbents for methylene blue removal

Amir Rabbi[a], Fatemeh Dadashian[a,*], Mansooreh Soleimani[b]

[a]*Department of Textile Engineering, Amirkabir University of Technology, Tehran, Iran, Tel. +982164542691; Fax: +982166400245; emails: dadashia@aut.ac.ir (F. Dadashian), Amir.rabbi@aut.ac.ir (A. Rabbi)*
[b]*Department of Chemical Engineering, Amirkabir University of Technology, Tehran, Iran, Tel. +982164543152; email: soleimanim@aut.ac.ir*

Received 12 July 2019; Accepted 29 September 2019

ABSTRACT

A novel microporous activated carbon fiber was prepared through thermal stabilization and chemical activation of acrylic fibers. BET, FESEM, and FTIR analysis were used to study different characteristics of the obtained adsorbent. Also, the iodine number, pH at point zero charge, and the mechanical properties of the samples were presented. The potential of this new adsorbent for removal of methylene blue (MB) from aqueous solution was studied in the batch experiments and the influence of main operating parameters including pH, initial dye concentration and adsorption time was studied. Relatively complete removal (about 95%) of MB dye was achieved at the pH of 12 and initial dye concentration of 100 mg/L. Moreover, it was revealed that the experimental data could be expressed well by the Langmuir and pseudo-second-order model, such that the maximum amount of monolayer adsorption was about 324.83 mg/g. The spontaneous and endothermic nature of the adsorption process was proved by thermodynamic parameters. This research revealed that, along with the pore filling mechanism, as the significant mechanism, the adsorption may have occurred via hydrogen bonding, n–π, π–π, and electrostatic interaction. Moreover, the desorption characteristics of the adsorbent were studied and about 86% desorption was achieved after three cycles. According to the results, the mechanical properties and adsorption/desorption capacity of this novel fabricated activated carbon fiber are relatively better than other adsorbents.

Keywords: Activated carbon fibers; Adsorption; Methylene blue; Isotherm; Kinetics

1. Introduction

In recent decades, treating wastewater to remove inorganic and organic contaminants has received much attention. Among the organic pollutants, the dyes have a large impact on contamination [1–3]. Methylene blue (MB), as one of the most famous basic dyes, can have many destructive effects on the health of human, therefore, it should be eliminated as much as possible [4].

There are different methods used to treat wastewater containing MB dyes; these include biological [5], chemical [6], and physical methods [7]. Among these methods, the physical adsorption by activated carbon, as a well-known adsorbent, can be very successful in removing pollutants [8–11]. Despite this, the fibrous forms of activated carbon, as compared with the conventional granular and powdered activated ones, have an enormous surface area, rapid adsorption/desorption rate and particular pore structures; as well, their ease of regeneration should be noted [12]. Activated carbon fibers (ACFs) are produced by physical and chemical activation process methods from the various types of synthetic [13–17] and natural fiber [18–21] precursors at temperatures generally higher than 500°C. Among these fibers, the acrylic fibers precursor is one of the most widely used

* Corresponding author.

materials because of its high carbon yield and relatively low price [12,22].

The adsorption features of MB on the activated carbon have been already well studied for a large number of purification and separation purposes [8,23–25]. Nevertheless, there are not many researches using the ACFs for this purpose. In Table 1, previous studies on the production methods and properties of ACFs have been reported.

In addition to the advantages mentioned for ACFs, they are expensive due to weight loss that they undergo during the activation process. As mentioned above, ACFs have a high adsorption/desorption rate and thus have a good recycling ability and can be used repeatedly and thus become more economical. But the low strength of these ACFs leads to its fragmentation and destruction during fluid passage and itself becomes a secondary source of pollutants. So, it is very important to find proper precursor fibers and suitable synthesis methods that can balance ACFs adsorption and mechanical properties [12]. Therefore, this study focused on the novel high adsorption/mechanical properties of acrylic-based activated carbon fibers (AACFs) which were fabricated chemically by KOH. The performance of this novel adsorbent was investigated to MB removal from aqueous solutions. The effects of main operating parameters including solution pH, temperature, and the initial dye concentration were investigated. Moreover, the equilibrium, kinetics, and thermodynamics of the adsorption process were studied. The possible mechanisms of MB adsorption on AACFs were also thoroughly studied.

2. Materials and methods

2.1. Fabrication of ACFs

The commercial acrylic fibers were purchased from Zhongfu Shenying carbon fiber Co. Ltd., China. AACFs were prepared by stabilizing the acrylic fibers in a stabilization oven under the air atmosphere at the temperature of 247°C for 140 min; after that, impregnation was done in 1.5 M KOH (purchased from Merck, Germany) aqueous solution bath with dwelling times about 30 min at 50°C; subsequently, they were activated in a furnace at the temperature of 800°C under 1% imposed stretch. In the activation stage, the temperature was enhanced progressively from 350°C to 800°C. At the end of the process, specimens were washed several times with HCl (5% w/w) and distilled water to eliminate the remaining KOH. These conditions produce an adsorbent with high adsorption/mechanical properties. Details of the effect of stabilization and activation parameters that led to the production of these new fibers with appropriate adsorption and mechanical properties were given in our previous paper [46]. The yield of the produced AACFs was estimated by considering the weight of the primary material and the weight of the produced AACFs.

2.2. Characterization of the obtained AACFs

Determination of the surface area and the distribution of pore diameter of the AACFs were done according to N_2 adsorption/desorption isotherms at 77 K using the Belsorp mini apparatus. The specimen had been outgassed about 8 h at 300°C before measurement. The apparent surface area was obtained with the BET model; then the pore size distribution was estimated based on the BJH method. Moreover, based on the amount of the N_2 that was adsorbed at the relative pressure (p/p_o) of ~0.98, the total pore volume was determined. The morphology of the AACFs was studied via field emission scanning electron microscopy (FESEM, Zeiss, Sigma VP, Germany).

In addition, the iodine number, which was described according to the amount of iodine adsorbed onto 1 g of AACFs, was estimated using the ASTM D 4607. It could be characteristic of the AACFs adsorption capacity along with their porosity [47].

Fourier transform infrared (FTIR, PerkinElmer Spectrum-65, with KBr pellet, Japan) spectroscopy was then employed to address the chemical structure of the specimen.

According to the BS ISO 11566 standard test method with a tensile-testing device, mechanical properties of the AACFs were calculated.

The pH at point zero charge (pH_{PZC}) was determined by salt addition method [48]. A solution of 0.01 M NaCl was used as the background electrolyte. 50 mL of this solution were apportioned into 11 flasks and the pH was maintained at 2, 3, 4, 5, 6, 7, 8, 9, 10, 11 and 12 by using 0.1 M NaOH or 0.1 M HCl solution where appropriate. Then, 0.2 g sample was added into all the flasks and agitated on a magnetic stirrer for 12 h at 25°C and the final pH values were recorded. pH_{PZC} value was identified at the pH when initial pH equals to the final pH.

2.3. Batch equilibrium studies

Adsorption experiments were performed as follows: 0.1 g of the AACFs were added into 150 mL Erlenmeyer flasks comprising 100 mL of dye solutions with various initial concentrations (50–400 mg/L). To reaching the equilibrium, the solutions were automatically stirred by employing a magnetic stirrer at 140 rpm for 300 min. The MB solution natural pH, namely 6, was selected to perform the equilibrium experiments. MB (Mw = 319 g/mol), as an adsorbate, provided by Merck. The dye concentrations, before adsorption and after equilibrium were measured at the maximum wavelength of 618 nm by means of a double beam UV/vis spectrophotometer (Shimadzu, Model UV 1601, Japan).

Various concentrations of dye solutions (i.e., 50, 100, 200, 300 and 400 mg/L) and time intervals (i.e., 10 to 300 min) were used to investigate the influence of the initial MB concentration on the AACFs adsorption. The adsorption capacity at equilibrium, q_e (mg/g), was calculated by Eq. (1).

$$q_e = \frac{\left(C_0 - C_e\right)V}{W} \tag{1}$$

In this equation, C_0 (mg/L) and C_e (mg/L) were the concentrations of MB at the initial and equilibrium time. In addition, V and W were the solution volume (L) and the AACFs dry mass (g), respectively.

Moreover, to explore the impact of the solution pH, a series of 100 mg/L MB solutions in different initial pH values from 2 to 12 were prepared by adding either HCl or NaOH;

Table 1
Previous studies on the fabrication methods and properties of ACFs

Adsorbent	Fabrication methods	Adsorbent properties	Characteristics	Descriptions	Ref.
PAN-based ACFs (2017)	Stabilization of 200 g/m^2 Felt: Air, 200°C, 50 min; then 300°C, 50 min Carbonization: argon, 1,000°C, 20 min Activation: CO_2, 1,000°C, 50 min	S_{BET}: 1,260 m^2/g V_{tot}: 0.59 cm^3/g Pore size: 1–2 nm	Burn off: 35% C content: 96% Crystallite size: 4.44 nm	- High surface area - Indirect activation - High burn off (low yield)	[26]
Lignin-based ACFs (2017)	Stabilization: Air, 200°C, 36 h Activation: N_2, 600°C, 90 min	S_{BET}: 117 m^2/g V_{tot}: 0.2 cm^3/g d_{avg}: 6.99 nm	Yield: 62%	- Low surface area - Very long time stabilization - Not significant water vapor adsorption - Improvement was done by using Fe_3O_4	[27]
PAN-based ACFs (2016)	Stabilization: air, 275°C, 30 min Carbonization: 600°C, 30 min Activation: CO_2, 900°C, 60 min	n.a.	D spacing (002): 0.218 nm Crystallite size: 1.286 nm	- The microstructure of the obtained ACFs was investigated	[28]
Waste cotton fiber-based ACFs (2016)	Activation: H_3PO_4 at 450°C, 0.5 h, impregnation ratio = 2	S_{BET}: 694 m^2/g V_{micro}: 0.288 cm^3/g MB adsorption: 344 mg/ g	C content: 89%	- High methylene blue adsorption capacity - 80.6% of the pore volume derives from the micropores - Fiber form was destroyed and final product was AC	[19]
Pitch-based ACFs (2015)	Stabilization: air, up to 240°C, 1 h Activation: KOH/fiber 3:1, 700°C, 1 h	S_{BET}: 1,720 m^2/g V_{tot}: 0.98 cm^3/g	Yield: 44%	- Direct activation of stabilized fiber - Reducing activating agent up to 70% - Final product: Short fiber	[29]
Modified commercial ACFs (2015)	Stabilization: mixture solution of Novolac, polyethylene glycol, and furfural coated on glass fiber and heated in air, 200°C, 4 h Activation/carbonization: N_2, 60 min	S_{BET}: 1,193 m^2/g V_{tot}: 0.58 cm^3/g Pore size: 2–4 nm MB adsorption: 45 mg/g	C content: 59% Tensile stress: 39.23 N E: 330.5 MPa D spacing (002): 0.360 nm Crystallite size: 1.608 nm	- High surface area - Low mechanical properties - Using extra-cost activation process to create more pores	[30]
Pitch-based ACFs (2014)	Stabilization: air, up to 240°C Activation: NaOH/Fiber 1:3, 900°C, 1 h	S_{BET}: 2,460 m^2/g V_{tot}: 1.34 cm^3/g d_{avg}: 2.02 nm	Yield: 17% Specific capacitance: up to 100 F g^{-1}	- High surface area - Direct activation - Reducing cost of production - Very low yield	[31]
Modified commercial ACF (2013)	Activation: KOH, 900°C, 60 min	S_{BET}: 2,318 m^2/g V_{tot}: 1.08 cm^3/g d_{avg}: 0.5–0.7 nm CO_2 adsorption: 176 mg/g	C content: 93%	- Using extra-cost activation process to create more pores - Final product: short fibers	[32]

(continued)

Table 1 *Continued*

Adsorbent	Fabrication methods	Adsorbent properties	Characteristics	Descriptions	Ref.
PAN-based ACFs (2012)	Stabilization: air, 275°C, 30 min Carbonization: 600°C, 60 min Activation: CO_2, 900°C, 60 min	S_{BET}: 672 m^2/g	n.a.	- Indirect activation - Nothing about mechanical properties	[33]
Acrylic waste-based ACFs (2012)	Pyrolysis: N_2, 700°C, Activation: steam, 900°C, 2 h	S_{BET}: 752 m^2/g V_{tot}: 0.4 cm^3/g	Burn off: 75%	- Precursor: cloth 2 cm^2 - Using waste fiber - Final product: not in fibrous form	[34]
Viscose-based ACFs (2012)	Impregnation of commercial ACF: 0.1 mol/L $Ni(NO_3)_2$ solutions; then dry at 75°C, 12 h Activation: $C_2H_2/H_2/N_2$ mixture gases, 550°C	Surface area: 435.78 m^2/g V_{micro}: 0.492 cm^3/g d_{avg}: 2 nm MB adsorption: 297 mg/g	n.a.	- By this fabrication method, CNTs were grown onto the surface of ACFs - Using extra-cost activation process to create more pores	[35]
Cotton-based ACF (2012)	Raw material impregnated in 95 g/L $ZnCl_2$, 1 h, then was sintered in argon at 500°C for 1 h	S_{BET}: 2,059 m^2/g MB adsorption: 597 mg/g Pore size: 1–2 nm	Yield: 37.6%	- Very high methylene blue adsorption - Fibrous form was destroyed	[36]
PAN-based AC (2010)	Stabilization: air, 195°C–280°C, 3–4 d then 400°C, 30 min Activation: steam, 800°C, 15 min	S_{BET}: 795 m^2/g V_{tot}: 0.407 cm^3/g d_{avg}: 2.05 nm Cu (II): 0.25 mmol/g Pb(II): 0.11 mmol/g	Yield: 13.8% C content: 69%	- Very long oxidation time - Very low carbon yield - Final product: not in fibrous form	[37]
Ultra-thin PAN-based ACFs (2008)	Stabilization: air, 280°C, 15 min Activation: steam, 1,000°C, 15 min	S_{BET}: 1,408 m^2/g V_{tot}: 0.782 cm^3/g d_{avg}: 2.22 nm	Burn off: 52.1% ρ: 2.18 g/cm^3 C content: 91%	- High density (Almost graphite density)	[38]
Pitch-based ACFs (2006)	Impregnation of commercial ACF: 0.5 mol/L $Ca(NO_3)_2$ solutions, vacuum, one day; then dry at 110°C, 1 d Activation: steam/argon, 850°C, 1 h	S_{BET}: 1,360 m^2/g V_{micro}: 0.39 cm^3/g V_{meso}: 0.46 cm^3/g d_{avg}: 0.7 nm MB adsorption: 295 mg/g	Burn off: 57%	- High surface area - The low burn-off ACF was used as a raw material - Very long fabrication method - Final product: short fiber - Using extra-cost activation process to create more mesopores	[39]
Porous carbon (PAN-based) (2004)	Activation of peroxidation cloth: KOH, 800°C, 30 min	S_{BET}: 3,000 m^2/g d_{avg}: 2 nm Benzene adsorption: 99% Iodine number: 1,700 mg/g	n.a.	- Very high adsorption properties - Low KOH ratio - Wide pore size distribution - Final product: not in fibrous form	[40]

Acrylic textile -based ACFs (2001)	Stabilization: N_2, 300°C, 2 h Carbonization: N_2, 800°C, 1 h Activation: CO_2, 900°C, 9 h	S_{BET}: 1,341.3 m^2/g V_{tot}: 0.6 cm^3/g d_{avg}: 1.278 nm	Burn off: 76% C content: 80% D spacing (002): 0.363 nm Crystallite size: 1.195 nm	- High surface area - Long time activation process - High burn-off (low yield) - Final product: short fiber	[41]
Acrylic-based activated carbon fabric (2000)	Stabilization: air, 250°C, 5 h Carbonization: sequential 9 stages in 900°C Activation: steam, 900°C, 5 min	Surface area: 2,400 m^2/g V_{tot}: 1.15 cm^3/g d_{avg}: 2.5–2.6 nm Iodine number: 1,800 mg/g Methylene blue adsorption: 300 mg/g Benzene adsorption: 54%	C content: 80%	- High surface area - High dye and iodine adsorption - High weight loss during the process - Long time carbonization stages	[42]
PAN-based ACFs (1995)	Stabilization: Air, 300°C, 2.25 h Activation: N_2/ CO_2, 900°C Regeneration: reactivation in CO_2, 900°C, 80 min	S_{BET}: 78.9 m^2/g Basic dye: 5 mg/g S_{BET} after four times regeneration: 972 m^2/g	C content: 74% σ: 600 MPa *E*: 120 GPa ρ: 1.72 g/cm^3 σ after four times regeneration: 450 MPa	- High mechanical properties before regeneration - Very low adsorption before regeneration - Long time process of regeneration - Reduction of mechanical properties after regeneration	[43]
PAN-based ACFs (1992)	Stabilization: Air, 300°C Carbonization/activation: N_2/CO_2, 900°C	Surface area: 276 m^2/g d_{avg}: 2.5- 2.6 nm Iodine number: 90.7 mg/g Basic blue 69 adsorption: 5.5 mg/g	C content: 74%	- Low surface area - Low dye and iodine adsorption	[44]
PAN-based ACFs (1987)	Stabilization: Air, 300°C Carbonization: 900°C Activation: steam/argon at 830°C for 1 h then vacuum at 850°C for 40 min then steam/argon 830°C for 30 min	S_{BET}: 815 m^2/g	C content: 85%	- Unknown stabilization and activation time - Very long time and complicated activation method	[45]

V_{tot}: Total pore volume (cm^3/g); d_{avg}: average pore diameter (nm); σ: tensile strength (MPa); *E*: Young modulus (GPa).

subsequently, the percentage removal of MB was estimated from Eq. (2).

$$\text{Dye Removal} = \frac{C_0 - C_e}{C_0} \times 100 \quad (2)$$

2.4. Adsorption isotherm

Adsorption isotherm models show how solutes can interact with the adsorbent. Four isotherm models, namely, Langmuir, Freundlich, Temkin and Dubinin–Radushkevich isotherms, were considered to check their capability in the description of the experimental data. Moreover, normalized standard deviation, $(\Delta q_e)\%$, which was determined by Eq. (3), and correlation coefficient (R^2) was utilized to estimate the validity of isotherm models.

$$\Delta q_e(\%) = \frac{\sqrt{\sum\left[\frac{\left(q_{e,\exp} - q_{e,\text{cal}}\right)}{q_{e,\exp}}\right]^2}}{N-1} \times 100 \quad (3)$$

In this equation, the experimental and calculated values of MB adsorption were indicated by $q_{e,\exp}$ (mg/g) and $q_{e,\text{cal}}$ (mg/g), respectively. Smaller (Δq_e) denotes that the model results can be compared with the experimental values.

2.5. Kinetic studies

Adsorption kinetics could serve as the measure of the adsorption uptake in terms of time. It is applied to measure the diffusion of adsorbate in the pores. In the study of adsorption, evaluation of the kinetic aspects should be done to further understand its mechanisms, features, and potentials of application. In order to define the residence time and to obtain the desired concentration of the adsorbate, kinetic data should be estimated, thereby helping to decide on the operation and design of adsorption apparatus [49]. The kinetic experiments were performed so that, sampling was done at specific time intervals and the dye concentration was determined. By using Eq. (4), q_t (mg/g), the amount of adsorption at time t, was determined.

$$q_t = \frac{\left(C_0 - C_t\right)V}{W} \quad (4)$$

In this equation, C_t (mg/L) was the obtained concentration of MB at certain time. In this section, the pseudo-first-order kinetic model and pseudo-second-order kinetic model were employed to probe the adsorption kinetics.

2.6. Thermodynamic study

For the evaluation of the thermodynamics of the adsorption process, $\Delta H°$, $\Delta S°$ and $\Delta G°$ were estimated as the three basic thermodynamic parameters, which, respectively, represented the standard enthalpy, standard entropy and standard free energy. In order to calculate the thermodynamic parameters, the equilibrium experiments were performed for 200 mg/L MB solution at 30°C, 40°C and 50°C.

2.7. Regeneration of the spent AACFs

For regeneration study, 0.1 g of adsorbent were contacted with 50 mg/L MB solution for 1 h using a magnetic stirrer. After equilibration, the MB concentration was determined. Then, the MB-loaded AACFs were agitated with the HCl (0.1 M) for 1 h. The amount of MB desorbed (% desorption) in each case was calculated by using Eq. (5).

$$\text{Desorption}(\%) = \frac{C_{\text{des}}}{C_{\text{ads}}} \times 100 \quad (5)$$

where C_{des} and C_{ads} (mg/L) represent the concentration of dye in desorbed and adsorbed phases, respectively. After each treatment, the adsorbent material was separated from the dye solution and washed with distilled water. The process was repeated for three cycles and desorption percentage was reported.

3. Results and discussion

3.1. Microstructural investigation of the produced ACFs

Figs. 1a and b display the surface morphology of the prepared AACFs. As it can be seen, the fibrous form of samples was entirely preserved. However, a certain amount of defects and flaws that were caused by activation have been observed. These defects actually shape the adsorption areas. Moreover, The FESEM photograph in Fig. 1b, demonstrated the wrinkles and a cracked morphology of the sample with some extended pores positioned randomly on the AACFs.

The characteristics of the fabricated AACFs including the specific surface area, total micropore volume, and the mesopore volume were presented in the previous work [46]. As it is shown in Table 2, The surface area of 561 m^2/g, V_{micro} of 0.2512 $cm^3\,g^{-1}$, and V_{meso} of 0.0542 $cm^3\,g^{-1}$ revealed that the obtained AACFs had formed a porous structure in a well shape, based on the BET analysis. In addition, it could be concluded from the BJH method that most of the pore sizes were in a range varying from 1.2 to 4.6 nm. Moreover, the average diameter of the pores was 2.736 nm. So, the AACFs included suitable regions for the adsorption of MB molecules. With the penetration of the KOH activating agent into the fiber structure during the impregnation and activation stage, the redox reactions took place in the fiber structure, which led to the formation of a porous structure. In this way, the KOH is reduced to metallic potassium and the carbon atoms in the fiber were oxidized to carbon monoxide and/or carbon dioxide. With the release of these gases from the surface of the sample, as well as severe metallic potassium outflow through the graphene layers, porosity was formed in the fibers [12].

As can be observed in Table 2, the tensile strength of the obtained AACFs was 431 MPa, which was adequate for manufacturing them in different shapes such as fabric, felt, etc. [50]. According to this data, the Young's modulus of these fibers was also high (51 GPa). The fiber modulus is directly related to the crystalline structure of the fibers and, unlike tensile strength, is less affected by structural defects [51]. Considering that the graphitic crystal structure was formed in the AACFs, these fibers had a relatively high modulus.

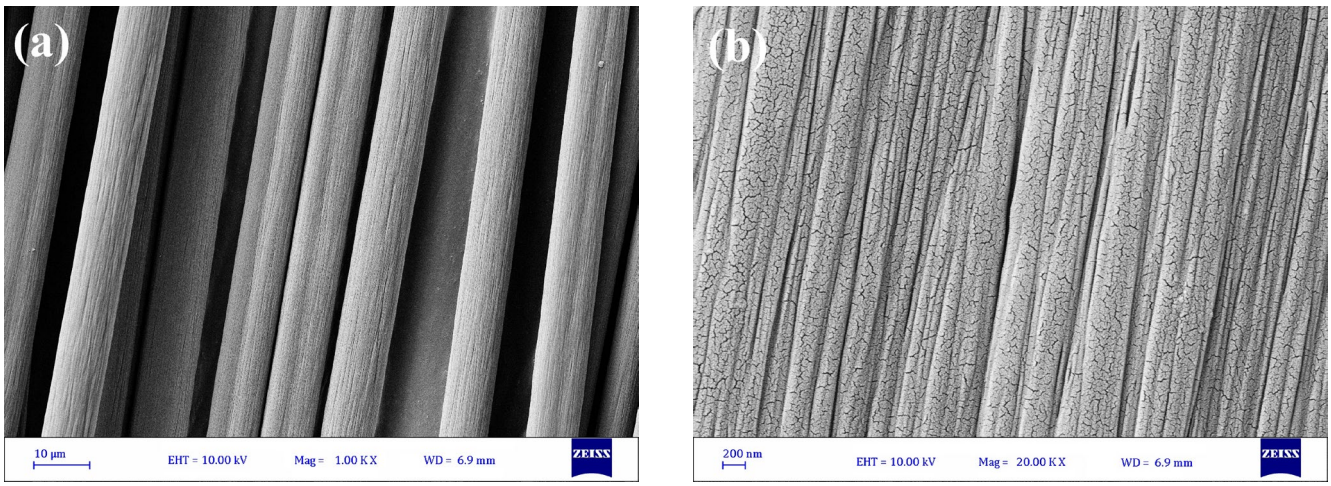

Fig. 1. FESEM photographs of the prepared AACF with various magnifications; (a) 1,000×, (b) 20,000×.

Table 2
Characteristics of the produced AACFs

Specific surface area, S_{BET}	561 m^2/g
V (mesopore)	0.0542 cm^3/g
V (micropore)	0.2512 cm^3/g
Average pore diameter	2.736 nm
Tensile strength	431 Mpa
Young's modulus	51 Gpa
Elongation	0.84%
Iodine adsorption	874 mg/g
Carbon yield	53%

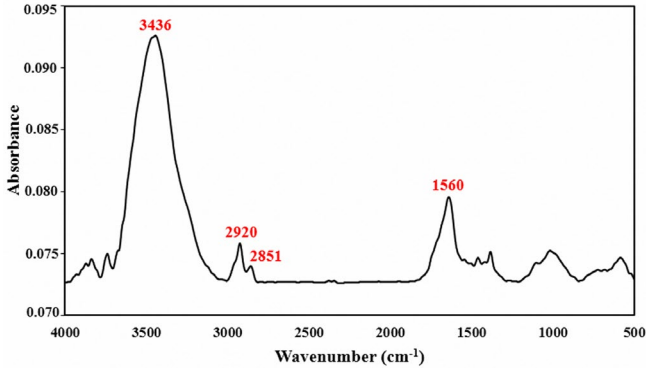

Fig. 2. FTIR spectrum of the produced sample.

Furthermore, the high iodine number of 874 mg/g indicated high adsorption capacity in the manufactured AACFs. Additionally, the high carbon yield value of 53% for the produced AACF could be more likely owing to the high carbon content of the acrylic precursor fibers [15]. Therefore, it can be concluded that the fabricated AACFs with an appropriate pore structure, proper tensile strength, high carbon yield and also high iodine adsorption can be applied effectively in the adsorption process.

In addition, the chemical structure of the produced AACFs is represented using the FTIR spectrum, as can be seen in Fig. 2. The peaks at 2,851 and 2,920 cm^{-1}, respectively, showed symmetric and asymmetric CH bonds [52]. An almost wide absorption peak at 3,436 cm^{-1} could be related to the bond stretching of the functional group of OH in the AACFs sample. Moreover, the absorption peak at 1,560 cm^{-1} was referred to the stretching mode of the aromatic ring [52]. So it could be regarded as an indicator of the development of aromatic structures in the graphite network which was shaped in the AACFs structure.

3.2. Effect of the solution pH

The influence of a pH range of 2–12 on the MB removal by the AACFs can be seen in Fig. 3. The solution pH serves as a significant parameter in the adsorbent surface chemistry [23]. Therefore, the amount of MB adsorption onto the AACFs surface could be affected through the pH of the solution. As shown in Fig. 3, by enhancing the value of pH, the MB removal percentage was improved, reaching a maximum of 95% at the pH of 12. In order to evaluate the effect of pH on the percentage of dye removal, the pH_{PZC} should be considered. The pH_{PZC} for the produced ACFs was measured approximately 4.3. In the acidic condition ($pH < pH_{PZC}$), there were more protons (H^+) in the solution. Due to competition between created H^+ and cationic MB molecules to adsorb into adsorbent sites, MB adsorption decreased. On the other hand, by enhancing the solution pH, the amount of negative sites on the surface of the AACFs increased, and as a consequence of electrostatic attraction, more MB cations were adsorbed. Similar results have been founded regarding the effects of pH on the MB adsorption by the cotton waste-based activated carbon [19] and activated carbons that had been obtained from the jute fiber [53].

3.3. Effect of the initial MB concentration

As can be seen in Fig. 4, the adsorbed MB onto AACFs was raised from 46.36 to 286.09 mg/g when the concentration of MB was enhanced from 50 to 400 mg/L. It can be attributed to the rise in the driving force generated by the concentration

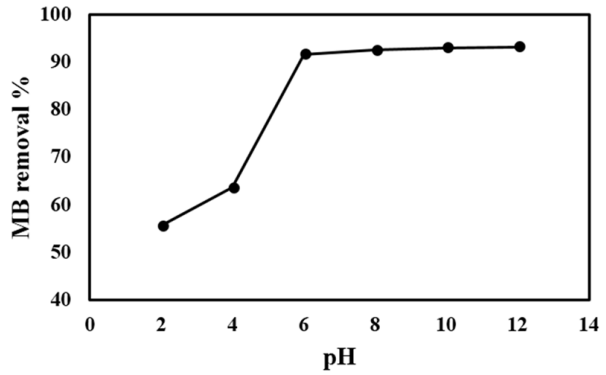

Fig. 3. Effect of initial solution pH on the adsorption of MB on the AACFs.

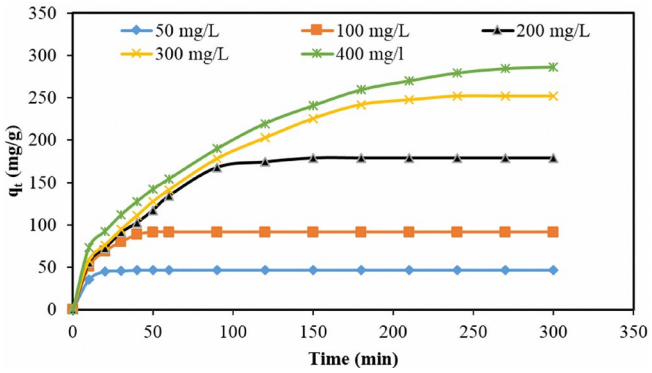

Fig. 4. Variation of adsorption capacity with adsorption time at various initial MB concentrations at 30°C and pH 6.

gradient, which, in turn, was due to the enhanced initial dye concentration [54]. As it was expected, the equilibrium of adsorption was obtained more quickly at the lower concentrations, as compared with the higher ones. The process of adsorption in the porous structure of AACFs involves some successive mass transfer steps which are gradual and take a relatively long time. So, AACFs could be efficient in adsorbing MBs from the aqueous solution and the process may get the equilibrium in a gradual manner, particularly in the case of higher initial dye concentrations.

3.4. Adsorption isotherms

To determine the adsorption isotherms of the MB dye on the AACFs, q_e against C_e was plotted and represented in Fig. 5. It could contribute to describing how dyes have interaction with ACFs, well as being essential in improving the usage of the adsorbents [23]. Therefore, four well-known isotherms including Langmuir, Freundlich, Temkin and Dubinin–Radushkevich (D–R) were employed to investigate the adsorption isotherms; these are explained in details below.

3.4.1. Langmuir isotherm

The linear form of the Langmuir isotherm model, which assumes that adsorption occurs on the surface of the adsorbent as a monolayer, is represented by Eq. (6) [55].

$$\frac{C_e}{q_e} = \frac{1}{K_L q_m} + \frac{1}{q_m} C_e \tag{6}$$

In this equation, Langmuir constants, that is, q_m and K_L, were the monolayer adsorption capacity and affinity of AACFs to MB, respectively. The K_L and q_m were estimated based on this isotherm and their values were displayed in Table 3. Verification of the experimental data into the Langmuir isotherm model can be seen in Fig. 5. It showed that MB molecules formed a monolayer coating on the surface of AACFs, which was the consequence of the AACFs surface homogeneity.

Moreover, the basic features of the Langmuir isotherm were obtained using equilibrium parameter of R_L [56], which was dimensionless and calculated via Eq. (7).

$$R_L = \frac{1}{1 + K_L C_0} \tag{7}$$

The calculated R_L values are displayed in Fig. 6. Considering the amount of R_L, it is possible to determine the isotherm type, which is unfavorable for $R_L > 1$, linear for $R_L = 1$, desirable for $0 < R_L < 1$ and is irreversible for $R_L = 0$. In this case, the R_L values were obtained in a range of 0.050–0.298, thereby confirming that the AACFs could be favorable for the MB dyes adsorption in the situations employed in this research.

3.4.2. Freundlich isotherm

The Freundlich isotherm, which deals with heterogeneous surfaces, shows that the adsorption is raised with the rise of concentration. The logarithmic form of Freundlich model [57] is represented in Eq. (8).

$$\log\left(q_e\right) = \log\left(K_F\right) + \frac{1}{n}\log\left(C_e\right) \tag{8}$$

In this equation, K_F ($mg^{1-c}\,L^c/g$, where $c = 1/n$) and $1/n$ were Freundlich constants, and were defined as adsorption capacity of the adsorbent and factor of heterogeneity, respectively. These constants were estimated from the plot of log q_e against log C_e, as tabulated in Table 3. The weak curve fitting in the diagram of q_e vs. C_e (Fig. 5) shows that the conditions of the Freundlich model were not satisfied. Moreover, as observed in Table 3, the value of 0.538 for $1/n$, which was less than one, indicated a regular Langmuir isotherm with a favorable adsorption [58].

3.4.3. Temkin isotherm

This isotherm assumes that the adsorption heat of whole molecules is decreased in linear form with the rise in coverage of the adsorbent surface; also, the adsorption is based on the uniform distribution of binding energies. The linear form of the Temkin isotherm model is presented in Eq. (9) [59].

$$q_e = \frac{RT}{b_T}\ln K_T + \frac{RT}{b_T}\ln C_e \tag{9}$$

Table 3
Langmuir, Freundlich, Temkin and D–R isotherm model parameters

Langmuir isotherm	
q_m (mg/g)	324.83
K_L (L/mg)	0.047
R_L	0.050
R^2	0.996
Δq_e	3.078
Freundlich isotherm	
$1/n$	0.538
K_f (mg^{1-c} L^c/g)	27.714
R^2	0.935
Δq_e	8.069
Temkin isotherm	
K_T (L/mg)	1.054
RT/b_T	74.116
R^2	0.983
Δq_e	38.627
D–R isotherm	
q_s (mg/g)	211.981
E (kJ/mol)	0.353
R^2	0.834
Δq_e	28.069

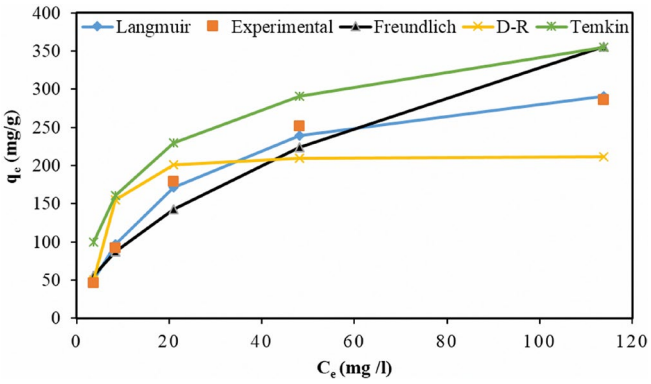

Fig. 5. Fit of different isotherms for MB adsorption on AACFs at 30°C and pH 6: the Langmuir, Freundlich, Temkin and D–R.

where K_T and RT/b_T were the equilibrium binding constant and the parameter represented to the adsorption heat, respectively. The Temkin isotherm and the associated parameters can be observed in Fig. 5 and Table 3.

3.4.4. Dubinin–Radushkevich isotherm

The Dubinin–Radushkevich (D–R) isotherm assumes that the adsorbent size is equivalent to the micropore dimension. It could provide information regarding the physical or chemical nature of adsorption processes. The D–R model [60] linear form is denoted by Eq. (10).

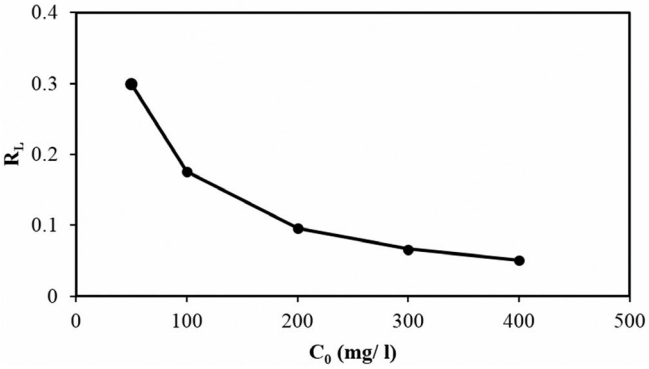

Fig. 6. Equilibrium parameter (R_L) for MB adsorption on AACFs.

$$\ln q_e = \ln q_s - \beta\varepsilon^2 \tag{10}$$

In this equation, q_e was the amount of MB adsorbed onto AACFs (mg/g) and, q_s was the maximum adsorption capacity (mg/g). The related parameters for the D–R model could yield by plotting ln q_e vs. ε^2, as presented in Table 3. Moreover, the adsorption potential (ε) could be estimated by employing Eq. (11).

$$\varepsilon = RT\ln\left(1+\frac{1}{C_e}\right) \tag{11}$$

The mean sorption free energy E (kJ/mol) could be yielded by employing Eq. (12) with the constant β (mol^2/J^2).

$$E = \left(\frac{1}{(2\beta)^{0.5}}\right) \tag{12}$$

In fact, the chemical or physical nature of the adsorption process was determined by the free energy (E). E values of 0.353 kJ/mol (a lesser amount of 8 kJ/mol) indicated that the physical adsorption was the process which was dominated in the adsorption of MB on AACFs.

According to the proposed isotherms in Fig. 5 and their related parameters in Table 3, it can be concluded that the MB adsorption by AACFs could be better described through the Langmuir model, since it provided the maximum value of R^2 (0.996) and the minimum value of Δq_e (3.078%), among the isotherm models examined in this study. Consequently, the mechanism of adsorption was homogeneous and monolayer, such that the maximum capacity of monolayer adsorption was 324.83 mg/g. The values of R^2 for the Temkin model were also relatively high, but its Δq_e values were higher than those estimated by the Langmuir model.

3.5. Comparison of ACF adsorbents for MB absorption

A large number of previous studies have come up with similar results, showing that the adsorption process of basic dye on the activated carbon was according to the Langmuir isotherm model [19,53,56]. Table 4 shows the comparison of the adsorption capacity of the ACFs to eliminate MB from

Table 4
Maximum adsorption capacity of some activated carbon fibers along with their operational conditions to eliminate MB from aqueous solutions

Adsorbent	pH	Temperature (°C)	Initial concentration	q_m (mg/g)	References
AACFs	6	30	50–400 mg/L	324.83	This work
Modified pitch-based ACFs	n.a.	27	5×10^{-6} mol/L	295	[39]
Activated carbon fiber	n.a.	27	50–100 mg/L	99.30	[61]
Jute fiber activated carbon	6	28	50–200 mg/L	225.64	[53]
Vegetal fiber activated carbons	6	30	20–100 mg/L	40	[62]
Resin-coated glass fiber–based ACF	n.a.	25	400 mg/L	45	[30]
Cotton-based ACF	7	RT	200–800 mg/L	597	[36]
Oil palm fiber activated carbon	6.5	30	50–500 mg/L	277.78	[63]
Piassava fibers activated carbon	n.a.	25	Up to 1,000 mg/L	276.40	[64]
Cotton-based activated carbon fibers	2–12	35	100–500 mg/L	476.19	[65]

aqueous solutions along with their operational conditions. As can be seen, the capacity of MB adsorption onto AACFs in this research (324.83 mg/g) was partly high in comparison with former adsorbents.

3.6. Adsorption kinetic models

To study the adsorption kinetics of the MB onto AACFs, two kinetic models of pseudo-first-order and pseudo-second-order were utilized. The pseudo-first-order model can be depicted via Eq. (13)[49].

$$\ln\left(q_e - q_t\right) = \ln q_e - k_1 t \tag{13}$$

In this equation, k_1 is referred to the adsorption rate constant (min^{-1}). As shown in Eq. (13), the slope of the graph of ln (q_e–q_t) vs. t, represented the value of k_1. This graph is presented in Fig. 7a. Moreover, the model parameters can be seen in Table 5.

In addition, the linear form of the pseudo-second-order adsorption model [49] can be expressed by Eq. (14).

$$\frac{t}{q_t} = \frac{1}{k_2 q_e^2} + \frac{1}{q_e} t \tag{14}$$

In this equation, k_2 (g mg^{-1} min) is referred to the constant of adsorption rate in this model. With respect to the slope and the intercept of the plots of t/q_t vs. t in Fig. 7b, the values of q_e and k_2 can be realized. As can be observed, a very good linear relationship was found in the plots. Moreover, the pseudo-second-order kinetic model parameters are tabulated in Table 5. Therefore, from Fig. 7b and Table 5, due to having relatively higher R^2 values, it can be concluded that the pseudo-second-order kinetic model, which proposed the chemical nature of the adsorption process, could match well over the entire range of discussed concentrations, thereby it could better characterize the adsorption kinetics [49].

3.7. Adsorption thermodynamics

It is known that in solid–liquid adsorption systems, from the changes occurring in the thermodynamic parameters including standard Gibbs free energy ($\Delta G°$), enthalpy ($\Delta H°$) and entropy ($\Delta S°$), we could confirm whether the adsorption is spontaneous, favorable, exothermic or endothermic [1]. To calculate the values of thermodynamic parameters, the Van't Hoff equation was applied, as shown below:

$$\ln k_d = \frac{-\Delta G°}{RT} = \frac{\Delta S°}{R} - \frac{\Delta H°}{RT} \tag{15}$$

R and T are the universal gas constant and the absolute temperature. k_d referred to the coefficient of distribution; k_d was obtained by the following equation:

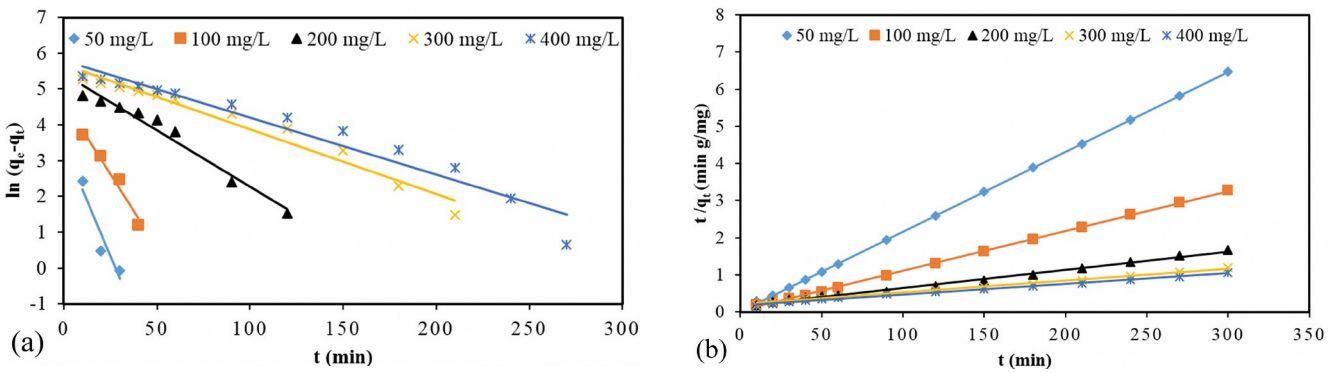

Fig. 7. Kinetics for adsorption of MB adsorption by AACFs at 30°C: (a) pseudo-first-order, (b) pseudo-second-order.

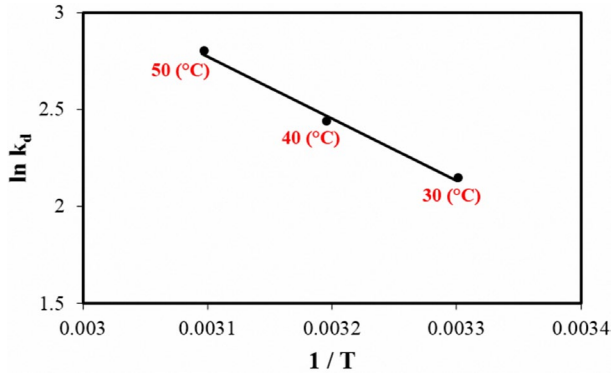

Fig. 8. Plot of ln K_d vs. 1/T (various temperatures).

$$k_d = \frac{q_e}{C_e} \tag{16}$$

Considering Fig. 8 and Eq. (15), it can be concluded that the slope of the graph of ln k_d vs. 1/T determines $\Delta H°$ and its intercept defines $\Delta S°$. It should be noted that, the equilibrium experiments were carried out at various temperatures for 200 mg/L MB solution. Table 6 shows the attained thermodynamic parameters.

The obtained negative $\Delta G°$ values revealed that the adsorption process was favorable and spontaneous; as well, by raising the temperature, the amount of the reaction spontaneity was increased. Moreover, the positive value of $\Delta S°$ was probably due to the enhanced mobility or excitement of MB at the interface of AACFs during the adsorption. In addition, the positive value of $\Delta H°$ implied the endothermic adsorption process.

3.8. Proposed adsorption mechanisms

As AACFs were porous materials with a large specific surface area, they can well adsorb MB molecules into their pores. Due to the low heat of adsorption (26.57 kJ/mol) and the low mean free energy, E (0.353 kJ/mol), it can be concluded that the most of adsorption could be expected to be physisorption. The pore filling mechanism was known as the main mechanism of the MB adsorption on AACFs. There are four possible interactions, as shown in Fig. 9. As can be observed in Fig. 9a, the hydroxyl group (H-donor) on AACFs can have bonds with nitrogen in MB (nitrogen is the H-acceptor atom). In addition, it is known that they can bond the aromatic rings in MB. The presence of the hydroxyl group on the AACFs surface has already been substantiated in the FTIR spectrum (Fig. 2). So hydrogen bonding could occur between MB and AACFs. This has also been reported for methyl orange and activated carbon [66].

Apart from the hydrogen bond, n–π interaction can also occur between O–H bonds or oxygen bonds on AACFs and the aromatic ring in MB, as can be seen in Fig. 9b. In these interactions, oxygen groups on the AACFs surface can serve as electron donors, whereas the aromatic rings of MB can behave as electron acceptors. The n–π interaction between the C–O group and the dye aromatic ring has been shown by Tran et al. [67].

Further, it was shown that there was π–π interaction between electrons of π (donor) in MB and electrons of π (acceptor) in AACFs, as can be seen in Fig. 9c. A large number of researches have also expressed similar interaction; they have described that what could occur between the dye and activated carbon is owing to the high amount of the aromatic ring in MB and activated carbons [67,68]. The aromatic rings in AACFs were identified via FTIR at 1,560 cm^{-1} (as can be seen in Fig. 2); so, the π–π interaction maybe occurred between MB and AACFs.

Eventually, the electrostatic interaction between MB and AACFs could contribute to the adsorption process. A special property of acrylic-based ACF is that it has nitrogen in its final structure [69]. So, it could serve as an adsorbent. As can be seen in Fig. 9d, the electronegative N-atom in the structure of AACFs could well electrostatically attract the positive cationic MB dye. The surface negative charge of the AACFs was owing to the presence of nitrogen-containing heteroatom

Table 5
Constants and regression coefficients for kinetic models of MB adsorption on AACFs

Initial MB concentration (mg/L)	$q_{e,exp}$ (mg/L)	Pseudo-first order parameters			Pseudo-second order parameters		
		$q_{e,cal}$ (mg/L)	k_1 (min^{-1})	R^2	$q_{e,cal}$ (mg/L)	$k_2 \times 10^3$ (g/mg min)	R^2
50	46.361	31.037	0.124	0.905	46.511	25.824	0.990
100	91.650	107.554	0.082	0.961	93.457	2.862	0.992
200	179.080	225.743	0.0314	0.967	204.081	0.163	0.994
300	251.849	296.189	0.0181	0.964	312.566	0.050	0.999
400	286.096	329.310	0.0159	0.944	344.827	0.046	0.999

Table 6
Thermodynamic parameters for MB adsorption onto prepared AACFs at different temperatures

Standard enthalpy $\Delta H°$ (kJ/mol)	Standard entropy $\Delta S°$ (kJ/mol K)	Gibbs free energy $\Delta G°$ (kJ/mol)		
		323 (K)	313 (K)	303 (K)
26.57	0.10	–7.52	–6.35	–5.41

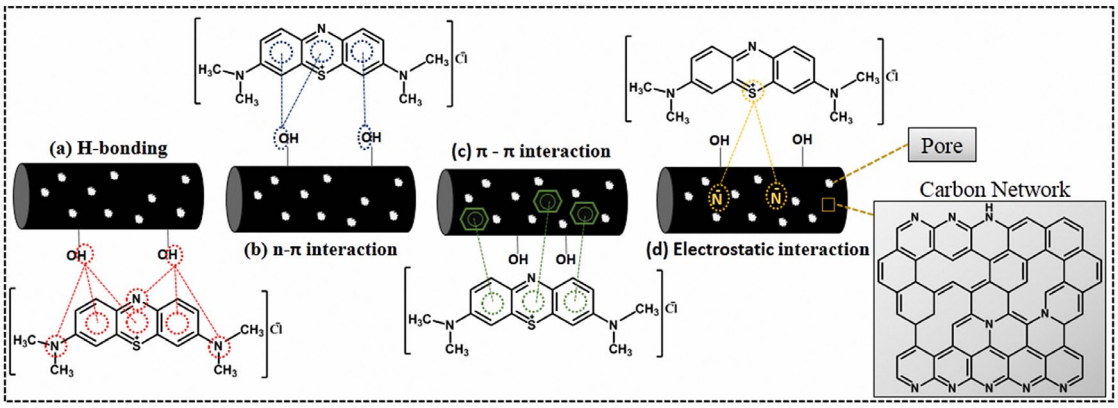

Fig. 9. Schematic of adsorption mechanisms of MB on AACFs surface through the interactions of (a) hydrogen bonding, (b) n–π bonding, and (c) π–π bonding, (d) electrostatic interaction.

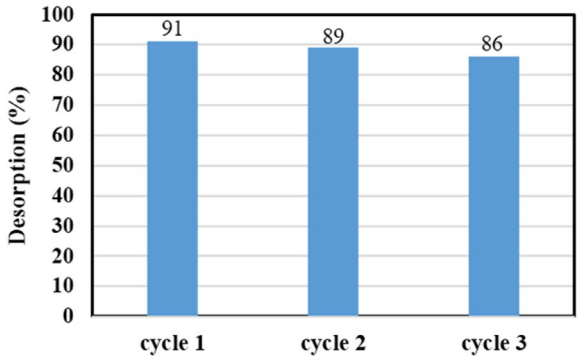

Fig. 10. Desorption efficiency of MB from AACFs for three cycles.

in the structure, leading to the interaction with cationic dye molecules.

3.9. Regeneration study

The important feature of an efficient adsorbent is its reusability with significant adsorption capacity and the regeneration of its original characteristics. The regeneration of the active sites on the spent adsorbent is proportional to its stability, which is essential for the industrial and large-scale practical applications. This will decrease the operational cost of the process as well as minimize the secondary pollution [1]. Thus an effective adsorbent must show excellent performance in the adsorption as well as in desorption processes. The desorption efficiency of produced AACFs was shown in Fig. 10. As it can be seen, around 91% of methylene blue was desorbed after the first desorption. The desorption efficiency of activated carbon was found to reduce gradually to 86% after three desorption cycles. Thus, it can be proposed that AACF is a stable and reusable adsorbent material and can be effectively used in a continuous flow system.

4. Conclusion

This study successfully prepared the acrylic-based ACF via stabilization and chemical activation of acrylic fiber. It was confirmed that the obtained high surface area AACFs were effective in MB elimination from aqueous solution. Moreover, it was demonstrated that MB adsorption was influenced by the pH of the initial solution and the initial MB concentrations. Also, it was found that the experimental data could be expressed well by using the Langmuir model, and the maximum monolayer adsorption capacity was achieved about 324.83 mg/g. According to kinetic data, the pseudo-second-order model with the highest value of R^2 was the best to describe the kinetics of MB adsorption onto AACFs. The determination of different thermodynamic parameters showed that the MB adsorption onto AACFs was feasible, spontaneous, and has endothermic nature. Although the pore filling mechanism was the main mechanism of dye adsorption on AACFs, the adsorption may have happened using hydrogen bonding, n–π interaction, π–π interaction and electrostatic interaction. Moreover, high desorption efficiency of 86% was achieved after three desorption cycles. According to the obtained results, it can be understood that the novel, high-performance reusable fibrous adsorbent materials produced in this study offer a great promise for the MB removal from industrial effluents, since, with increasing the mechanical properties of ACFs, their resistance to fluid passage increases and thus their performance improves significantly compared with conventional adsorbents.

Symbols

q_e — Amount of adsorption at equilibrium, mg/g
C_0 — Concentrations of dye at initial, mg/L
C_e — Concentrations of dye at equilibrium, mg/L
V — Volume of the solution, L
W — Mass of dry adsorbent, g
R^2 — Correlation coefficient
Δq_e — Normalized standard deviation, %
$q_{e,\text{exp}}$ — Experimental values for the amount of dyes adsorbed, mg/g
$q_{e,\text{cal}}$ — Calculated values for the amount of dyes adsorbed, mg/g
q_t — Amount of adsorption at the time t, mg/g
C_t — Concentration of dye at the time t, mg/L
q_m — Maximum monolayer adsorption capacity, mg/g

K_L — Langmuir isotherm constant, L/mg
R_L — Dimensionless equilibrium parameter
n — Freundlich isotherm constant, heterogeneity factor
K_f — Freundlich isotherm constant, adsorption capacity ($mg^{1-c} L^c/g$), where $c = 1/n$
K_T — Equilibrium binding constant, L/mg
T — Temperature in Kelvin, K
R — Universal gas constant, 8.314 J/mol K
q_s — Maximum adsorption capacity in D–R isotherm
E — Free energy, kJ/mol
β — D–R isotherm constant, mol^2/J^2
ε — Adsorption potential
k_1 — Rate constant of pseudo-first-order adsorption, min^{-1}
k_2 — Rate constant of pseudo-second-order adsorption, g/mg min
k_d — Distribution coefficient
$\Delta H°$ — Standard enthalpy, kJ/mol
$\Delta S°$ — Standard entropy, kJ/mol K
$\Delta G°$ — Standard Gibbs free energy, kJ/mol
C_{des} — Concentration of dye in desorbed phases
C_{ads} — Concentration of dye adsorbed phases

References

[1] A. Bonilla-Petriciolet, D.I. Mendoza-Castillo, H.E. Reynel-Ávila, Adsorption Processes for Water Treatment and Purification, 1st ed., Springer International Publishing, Cham, 2017.
[2] C. Fernández, M.S. Larrechi, M.P. Callao, An analytical overview of processes for removing organic dyes from wastewater effluents, TrAC - Trends Anal. Chem., 29 (2010) 1202–1211.
[3] K.Y. Foo, B.H. Hameed, An overview of dye removal via activated carbon adsorption process, Desal. Wat. Treat., 19 (2010) 255–274.
[4] V. Vadivelan, K. Vasanth Kumar, Equilibrium, kinetics, mechanism, and process design for the sorption of methylene blue onto rice husk, J. Colloid Interface Sci., 286 (2005) 90–100.
[5] A. Machrouhi, M. Farnane, A. Elhalil, M. Abdennouri, H. Tounsadi, S. Qourzal, N. Barka, Biosorption potential of *Thapsia transtagana* stems for the removal of dyes: kinetics, equilibrium and thermodynamics, Desal. Wat. Treat., 126 (2018) 324–332.
[6] T. Zhang, Z.R. Nan, Decolorization of Methylene Blue and Congo Red by attapulgite-based heterogeneous Fenton catalyst, Desal. Wat. Treat., 57 (2016) 4633–4640.
[7] B. Fryczkowska, The application of ultrafiltration composite GO/PAN membranes for removing dyes from textile wastewater, Desal. Wat. Treat., 128 (2018) 79–88.
[8] M. Rafatullah, O. Sulaiman, R. Hashim, A. Ahmad, Adsorption of methylene blue on low-cost adsorbents: a review, J. Hazard. Mater., 177 (2010) 70–80.
[9] R.C. Bansal, M. Goyal, Activated Carbon Adsorption, 1st ed., CRC Press, 2005.
[10] K.J.L. dos Santos, G.E. de Souza dos Santos, Í.M.G.L. de Sá, S.H.V. de Carvalho, J.I. Soletti, L. Meili, J.L. da Silva Duarte, M.D. Bispo, G.L. Dotto, *Syagrus oleracea*–activated carbon prepared by vacuum pyrolysis for methylene blue adsorption, Environ. Sci. Pollut. Res., 26 (2019) 16470–16481.
[11] N. Mehrabi, M. Soleimani, M.M. Yeganeh, H. Sharififard, Parameter optimization for nitrate removal from water using activated carbon and composite of activated carbon and Fe_2O_3 nanoparticles, RSC Adv., 5 (2015) 51470–51482.
[12] J.Y. Chen, Activated Carbon Fiber and Textiles, 1st ed., Elsevier, 2017.
[13] Z. Yue, A. Vakili, J. Wang, Activated carbon fibers from melt-blown isotropic pitch fiber webs for vapor phase adsorption of volatile organic compounds, Chem. Eng. J., 330 (2017) 183–190.
[14] J.P. Boudou, P. Parent, F. Suárez-García, S. Villar-Rodil, A. Martínez-Alonso, J.M.D. Tascón, Nitrogen in aramid-based activated carbon fibers by TPD, XPS and XANES, Carbon N. Y., 44 (2006) 2452–2462.
[15] B. Maddah, K. Nasouri, Fabrication of high surface area PAN-based activated carbon fibers using response surface methodology, Fibers Polym., 16 (2015) 2141–2147.
[16] H.M. Feng, S.J. Zhang, Y.Z. Chen, Y.W. Ding, H.Q. Yu, M.H.W. Lam, Fabrication and evaluation of mesoporous poly(vinyl alcohol)-based activated carbon fibers, Ind. Eng. Chem. Res., 48 (2009) 3398–3402.
[17] M. Vujković, L. Matović, J. Krstić, M. Stojmenović, A. Đukić, B. Babić, S. Mentus, Mechanically activated carbonized rayon fibers as an electrochemical supercapacitor in aqueous solutions, Electrochim. Acta, 245 (2017) 796–806.
[18] E. Ekrami, F. Dadashian, M. Soleimani, Waste cotton fibers based activated carbon: optimization of process and product characterization, Fibers Polym., 15 (2014) 1855–1864.
[19] E. Ekrami, F. Dadashian, M. Arami, Adsorption of methylene blue by waste cotton activated carbon: equilibrium, kinetics, and thermodynamic studies, Desal. Wat. Treat., 57 (2016) 7098–7108.
[20] R. Salehi, F. Dadashian, M. Abedi, B. Hasani, Optimization of chemical activation of cotton fabrics for activated carbon fabrics production using response surface methodology, J. Text. Inst., 109 (2018) 1586.
[21] J.M. Huang, I.J. Wang, C.H. Wang, Preparation and adsorptive properties of cellulose-based activated carbon tows from cellulose filaments, J. Polym. Res., 8 (2001) 201–207.
[22] P.J.M. Carrott, M.M.L. Ribeiro Carrott, P.F.M.M. Correia, Evolution of porosity of activated carbon fibres prepared from pre-oxidized acrylic fibres, Microporous Mesoporous Mater., 264 (2018) 176–180.
[23] M.T. Yagub, T.K. Sen, S. Afroze, H.M. Ang, Dye and its removal from aqueous solution by adsorption: a review, Adv. Colloid Interface Sci., 209 (2014) 172–184.
[24] A.H. Jawad, M.H. Sauodi, M.S. Mastuli, M.A. Aouda, K.A. Radzun, Pomegranate peels collected from fresh juice shop as a renewable precursor for high surface area activated carbon with potential application for methylene blue adsorption, Desal. Wat. Treat., 124 (2018) 287–296.
[25] M. Pirsaheb, Z. Rezai, A.M. Mansouri, A. Rastegar, A. Alahabadi, A.R. Sani, K. Sharafi, Preparation of the activated carbon from India shrub wood and their application for methylene blue removal: modeling and optimization, Desal. Wat. Treat., 57 (2016) 5888–5902.
[26] M.A. do Amaral Junior, J.T. Matsushima, M.C. Rezende, E.S. Gonçalves, J.S. Marcuzzo, M.R. Baldan, Production and characterization of activated carbon fiber from textile PAN Fiber, J. Aerosp. Technol. Manage., 9 (2017) 423–430.
[27] M. Song, W. Zhang, Y. Chen, J. Luo, J.C. Crittenden, The preparation and performance of lignin-based activated carbon fiber adsorbents for treating gaseous streams, Front. Chem. Sci. Eng., 11 (2017) 328–337.
[28] N. Yusof, D. Rana, A.F. Ismail, T. Matsuura, Microstructure of polyacrylonitrile-based activated carbon fibers prepared from solvent-free coagulation process, J. Appl. Res. Technol., 14 (2016) 54–61.
[29] N. Díez, P. Álvarez, M. Granda, C. Blanco, R. Santamaría, R. Menéndez, A novel approach for the production of chemically activated carbon fibers, Chem. Eng. J., 260 (2015) 463–468.
[30] X.Q. Wei, Q.H. Li, H.C. Li, H.J. Li, S.X. Chen, The use of $ZnCl_2$ activation to prepare low-cost porous carbons coated on glass fibers using mixtures of Novolac, polyethylene glycol and furfural as carbon precursors, Xinxing Tan Cailiao/New Carbon Mater., 30 (2015) 579–586.
[31] N. Diez, P. Díaz, P. Álvarez, Z. González, M. Granda, C. Blanco, R. Santamaría, R. Menéndez, Activated carbon fibers prepared directly from stabilized fibers for use as electrodes in supercapacitors, Mater. Lett., 136 (2014) 214–217.
[32] S.Y. Lee, S.J. Park, Determination of the optimal pore size for improved CO_2 adsorption in activated carbon fibers, J. Colloid Interface Sci., 389 (2013) 230–235.

[33] N. Yusof, A.F. Ismail, D. Rana, T. Matsuura, Effects of the activation temperature on the polyacrylonitrile/acrylamide-based activated carbon fibers, Mater. Lett., 82 (2012) 16–18.
[34] M.A. Nahil, P.T. Williams, Surface chemistry and porosity of nitrogen-containing activated carbons produced from acrylic textile waste, Chem. Eng. J., 184 (2012) 228–237.
[35] L. Wang, Z. Huang, M. Zhang, B. Chai, Adsorption of methylene blue from aqueous solution on modified ACFs by chemical vapor deposition, Chem. Eng. J., 189–190 (2012) 168–174.
[36] K.L. Chiu, D.H.L. Ng, Synthesis and characterization of cotton-made activated carbon fiber and its adsorption of methylene blue in water treatment, Biomass Bioenergy, 46 (2012) 102–110.
[37] M.A.A. Zaini, Y. Amano, M. Machida, Adsorption of heavy metals onto activated carbons derived from polyacrylonitrile fiber, J. Hazard. Mater., 180 (2010) 552–560.
[38] Y.J. Su, T.H. Ko, J.H. Lin, Preparation of ultra-thin PAN-Based activated carbon fibers with physical activation, J. Appl. Polym. Sci., 108 (2008) 3610–3617.
[39] S. Lei, J. ichi Miyamoto, H. Kanoh, Y. Nakahigashi, K. Kaneko, Enhancement of the methylene blue adsorption rate for ultramicroporous carbon fiber by addition of mesopores, Carbon N. Y., 44 (2006) 1884–1890.
[40] M. Wu, Q. Zha, J. Qiu, Y. Guo, H. Shang, A. Yuan, Preparation and characterization of porous carbons from PAN-based preoxidized cloth by KOH activation, Carbon N. Y., 42 (2004) 205–210.
[41] P.J.M. Carrott, J.M.V. Nabais, M.M.L. Ribeiro Carrott, J.A. Pajares, Preparation of activated carbon fibres from acrylic textile fibres, Carbon N. Y., 39 (2001) 1543–1555.
[42] S.Y. You, Y.H. Park, C.R. Park, Preparation and properties of activated carbon fabric from acrylic fabric waste, Carbon N. Y., 38 (2000) 1453–1460.
[43] T.H. Ko, Regeneration of PAN-based activated carbon fibers by thermal treatments in air and carbon dioxide, J. Mater. Res., 10 (1995) 1969–1976.
[44] T.H. Ko, P. Chiranairadul, C.H. Lin, The study of polyacrylonitrile-based activated carbon fibres for water purification: Part I, J. Mater. Sci. Lett., 11 (1992) 6–8.
[45] P.H. Wang, K.L. Hong, Q.R. Zhu, Surface analyses of polyacrylonitrile-based activated carbon fibers by X-ray photoelectron spectroscopy, J. Appl. Polym. Sci., 62 (1996) 1987–1991.
[46] A. Rabbi, F. Dadashian, Simultaneous improvement in tensile strength and adsorption capacity of activated carbon fibers during stabilization and activation of acrylic fibers, Diam. Relat. Mater., 95 (2019) 174–184.
[47] A. Mianowski, M. Owczarek, A. Marecka, Surface area of activated carbon determined by the iodine adsorption number, Energy Sources, Part A, 29 (2007) 839–850.
[48] T. Mahmood, A. Khan, A. Naeem, M. Hamayun, M. Muska, M. Farooq, F. Hussain, Adsorption of Ni(II) ions from aqueous solution onto a fungus *Pleurotus ostreatus*, Desal. Wat. Treat., 57 (2016) 7209–7218.
[49] L. Largitte, R. Pasquier, A review of the kinetics adsorption models and their application to the adsorption of lead by an activated carbon, Chem. Eng. Res. Des., 109 (2016) 495–504.
[50] M. Yoshida, M. Hirai, Process for Production of Activated Carbon, US Patent, US4256607A, 1981.
[51] J.W.S. Hearle, W.E. Morton, Physical Properties of Textile Fibres, Fourth edition, Woodhead publishing limited, Cambridge, 2008.
[52] A.A. Spagnoli, D.A. Giannakoudakis, S. Bashkova, Adsorption of methylene blue on cashew nut shell based carbons activated with zinc chloride: The role of surface and structural parameters, J. Mol. Liq., 229 (2017) 465–471.
[53] S. Senthilkumaar, P.R. Varadarajan, K. Porkodi, C.V. Subbhuraam, Adsorption of methylene blue onto jute fiber carbon: kinetics and equilibrium studies, J. Colloid Interface Sci., 284 (2005) 78–82.
[54] M. Aseel, N. Abbas, F. Ayad, Kinetics and equilibrium study for the adsorption of textile dyes on coconut shell activated carbon, Arab. J. Chem., 10 (2017) S3381–S3393.
[55] I. Langmuir, The constitution and fundamental properties of solids and liquids. Part I Solids, J. Am. Chem. Soc., 38 (1916) 2221–2295.
[56] I.A.W. Tan, A.L. Ahmad, B.H. Hameed, Enhancement of basic dye adsorption uptake from aqueous solutions using chemically modified oil palm shell activated carbon, Colloids Surf., A, 318 (2008) 88–96.
[57] H.M.F. Freundlich, Over the adsorption in solution, J. Phys. Chem, 57 (1906) 385–471.
[58] C. Senthamarai, P.S. Kumar, M. Priyadharshini, P. Vijayalakshmi, V.V. Kumar, P. Baskaralingam, K.V. Thiruvengadaravi, S. Sivanesan, Adsorption behavior of methylene blue dye onto surface modified *Strychnos potatorum* seeds, Environ. Prog. Sustain. Energy, 32 (2013) 624–632.
[59] M.J. Temkin, V. Pyzhev, Recent modifications to Langmuir isotherms, Acta Physiochem. USSR, 12 (1940) 217–225.
[60] M.M. Dubinin, L.V. Radushkevich, Equation of the characteristics curves of activated charcoal, Proc. Acad. Sci. USSR. Phys. Chem. Sect., 55 (1947) 331–333.
[61] Y. Zhi-Yuan, Kinetics and mechanism of the adsorption of methylene blue onto ACFs, J. China Univ. Min. Technol., 18 (2008) 0437–0440.
[62] H. Cherifi, B. Fatiha, H. Salah, Kinetic studies on the adsorption of methylene blue onto vegetal fiber activated carbons, Appl. Surf. Sci., 282 (2013) 52–59.
[63] I.A.W. Tan, B.H. Hameed, A.L. Ahmad, Equilibrium and kinetic studies on basic dye adsorption by oil palm fibre activated carbon, Chem. Eng. J., 127 (2007) 111–119.
[64] F.F. Avelar, M.L. Bianchi, M. Gonçalves, E.G. da Mota, The use of piassava fibers (*Attalea funifera*) in the preparation of activated carbon, Bioresour. Technol., 101 (2010) 4639–4645.
[65] X. Duan, C. Srinivasakannan, X. Wang, F. Wang, X. Liu, Synthesis of activated carbon fibers from cotton by microwave induced H_3PO_4 activation, J. Taiwan Inst. Chem. Eng., 70 (2017) 374–381.
[66] R.-S. Juang, Y.-C. Yei, C.-S. Liao, K.-S. Lin, H.-C. Lu, S.-F. Wang, A.-C. Sun, Synthesis of magnetic Fe_3O_4/activated carbon nanocomposites with high surface area as recoverable adsorbents, J. Taiwan Inst. Chem. Eng., 90 (2018) 51–60.
[67] H.N. Tran, Y.F. Wang, S.J. You, H.P. Chao, Insights into the mechanism of cationic dye adsorption on activated charcoal: the importance of Π–Π interactions, Process Saf. Environ. Prot., 107 (2017) 168–180.
[68] M. Ji, S. ShuangShuang, C. KeZheng, Facile and scalable synthesis of magnetite/carbon adsorbents by recycling discarded fruit peels and their potential usage in water treatment, Bioresour. Technol., 233 (2017) 110–115.
[69] M. Suzuki, Activated carbon fiber: Fundamentals and applications, Carbon N. Y., 32 (1994) 577–586.